

Spectroscopy of terahertz radiation using high- Q photonic crystal microcavities

V. M. Muravev, P. A. Gusikhin, G. E. Tsydynzhapov, A. A. Fortunatov, and I. V. Kukushkin
Institute of Solid State Physics, RAS, Chernogolovka 142432, Russia and
Terasense Development Laboratories, Chernogolovka 142432, Russia

(Received 11 September 2012; revised manuscript received 10 November 2012; published 27 December 2012)

We report observation of high- Q resonance in the photoresponse of a detector embedded in the 2D photonic crystal slab (PCS) microcavity illuminated by terahertz radiation. The detector and PCS are fabricated from a single GaAs wafer in a unified process. The influence of the period of PCS lattice, microcavity geometry, and detector location on the resonant photoresponse is studied. The resonance is found to originate from coupling of the fundamental PCS microcavity photon mode to the detector. The phenomenon can be exploited to devise a spectrometer-on-a-chip for terahertz range.

DOI: [10.1103/PhysRevB.86.235144](https://doi.org/10.1103/PhysRevB.86.235144)

PACS number(s): 42.50.-p, 42.70.Qs, 42.79.-e, 73.21.-b

Recent years have witnessed a surge of research activity in the field of terahertz radiation (100 GHz to 3 THz). In part, such interest is caused by unique properties of THz radiation, which foretell a variety of potential applications.¹ However, its spectral location between optical and microwave frequencies hinders development of compact THz generation and spectroscopic systems. This leads to an increased need for components that can be used to manipulate THz radiation on-chip. However, in comparison with electrons in media, it is difficult to confine or store light and to control its speed. Photonic crystals (PCs) are expected to solve the problems by letting one manipulate the behavior of light in media beyond the conventional limitations.²⁻⁴ However, at present photonics is not versatile enough, and many standard electronic functions such as memory and logic cannot be achieved by THz photonics alone. For this reason, research on hybrid photonic crystal–electronic structures is of great importance.

Early experiments on THz PCs have primarily focused on defect-free structures.^{5,6} Their main objective was to investigate properties of periodic media in a regime where fabrication was less challenging than at optical frequencies. However, it is clear that just as at optical frequencies, the utility of THz photonic crystals relies on the incorporation of defects to disturb the periodicity and thereby introduce localized cavity photon modes.^{7,8} The first terahertz experiments on PCs with embedded defects have demonstrated the existence of a high- Q photon cavity mode.⁹⁻¹³ Research on hybrid PC–electronic devices was pioneered in the works of electrically pumped photonic-crystal THz quantum cascade lasers.^{14,15} The application of PC technology has enabled simultaneous spectral and spatial laser mode engineering.

In the present work we realize a hybrid PC–electronic THz detector system in a unified lithographic process. We study its properties and find a frequency selectivity with a quality factor of up to $Q = 210$, which opens possibilities for a “spectrometer-on-a-chip” for the sub-THz and THz frequency ranges.

A broadband detector and two-dimensional (2D) photonic crystal slab (PCS) consisting of a triangular lattice of air holes were fabricated from a single GaAs wafer with embedded GaAs/AlGaAs heterostructure. The wafer had a 20 nm single quantum well located 200 nm below the top crystal surface. Room temperature electron density was $n_s = 6 \times 10^{11} \text{ cm}^{-2}$ with corresponding mobility $6000 \text{ cm}^2/\text{V s}$. The detector was

placed inside a microcavity composed of three linearly aligned missing air holes (defined as L3) [Fig. 1(a)]. The detector operation principle relied on coupling of incident terahertz radiation to the metallic detector gates that triggers plasma waves in the two-dimensional electron system (2DES). An ac plasmon potential was then rectified into dc photovoltage on the nonlinear defect introduced in the 2DES. The fabrication process was as follows. First, an ordinary optical lithography procedure was performed to fabricate the detector on the top crystal side. Details of the detector geometry can be found elsewhere.^{16,17} Then the wafer was thinned down to a thickness of $h = 200 \text{ }\mu\text{m}$. After that, anisotropic deep reactive ion etching in the chlorine atmosphere was used to produce pass-through holes to form the PC. The etching was performed from the bottom side of the wafer to protect the detector. The resulting structure and wafer cross-section are shown in Figs. 1(a) and 1(b). PCSs have been made with triangular lattice constants $a = 247, 292, 343, 374, 411, 544,$ and $816 \text{ }\mu\text{m}$. The diameter of holes was $d = 0.6a$, total sample size $6 \times 6 \text{ mm}^2$. Also, a reference sample of the same size and with the same detector but no PC (therefore, broadband) have been produced. Samples have been fixed by corners on a chip carrier with a through cut under the region of the photonic crystal [Figs. 1(c) and 1(d)]. To measure frequency response of the detector we used a set of tunable backward-wave oscillators operating in the frequency range 0.1 to 0.4 THz and generating continuous wave radiation with typical output power from 10 to 0.1 mW. The radiation was collimated into the parallel beam of 1 cm diameter and directed onto the sample perpendicularly to the PCS plane. The radiation was chopped at 25 Hz frequency, and photoresponse of the detector was measured synchronously at the same frequency. The measurements were carried out at room temperature.

Figure 2 shows frequency dependence of photoresponse of the detector for two different samples. The bottom curve corresponds to the reference sample without photonic crystal. Signal modulation arises from interference of the standing electromagnetic waves inside the GaAs crystal, which acts as a resonator. The upper and middle curves display the photoresponse of the detector embedded in the L3 microcavity in the PCS with a period of $a = 411 \text{ }\mu\text{m}$. The sample was irradiated from the back side. One curve was measured under the incident THz radiation with longitudinal polarization (E field along the microcavity axis), while another used transverse

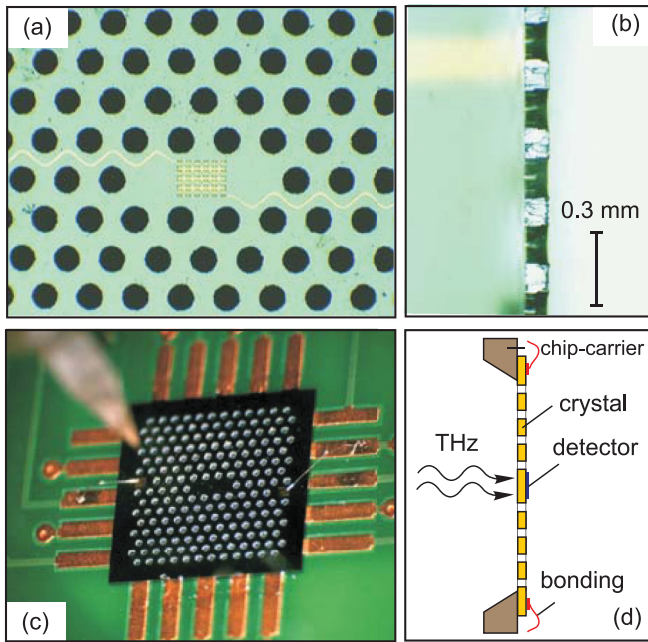


FIG. 1. (Color online) (a) Microscopy image of L3 PC microcavity with embedded detector. The PC triangular lattice constant is $a = 292 \mu\text{m}$, and the slab thickness is $h = 200 \mu\text{m}$. (b) Cross section of the PC. (c) Chip carrier with mounted PC. There is a square hole in the chip carrier under the entire PC surface. (d) Side view of chip carrier and sample.

polarization. The curves were offset vertically for clarity. The presence of the photonic crystals results in suppression of most of the peaks related to internal reflections in the sample since no electromagnetic wave can propagate along its surface inside the stop band of the PC. It also gives rise to a sharp peak at the frequency $f = 215 \text{ GHz}$ with quality factor up to $Q = 150$, which is due to the resonance inside the microcavity. To explain why we observe resonance only in the polarization direction along the long side of the PCS microcavity, though resonances for both are expected in our frequency range, we performed numeric simulation of the electromagnetic field profile inside the microcavity dielectric slab. Two inset panels show maps of electric field amplitude in the longitudinal cross-section of the PCS ($a = 411 \mu\text{m}$) in longitudinal (right panel) and transverse (left panel) polarization directions at resonant point. The thick black line indicates the position of the detector in the microcavity. In both cases a parallel THz beam with unitary power was directed onto the back (bottom) side of the sample [Fig. 1(d)]. It is found that for the transverse polarization the field central lobe is shifted towards the back part of the crystal side, whereas in the longitudinal polarization the lobe is much stronger and is shifted towards the top surface, where the detector is located.

Figure 3 shows photoresponse of the terahertz detector in PC slabs with lattice constants $a = 411 \mu\text{m}$, $374 \mu\text{m}$, and $343 \mu\text{m}$ for longitudinal polarization. The resonance frequency position (marked by arrows) shifts with PCS period a . The inset of Fig. 2 shows positions of the resonances as a function of the inverse lattice constant. The solid line represents theoretical prediction calculated using the finite difference time domain (FDTD) simulations. There is a good agreement between the

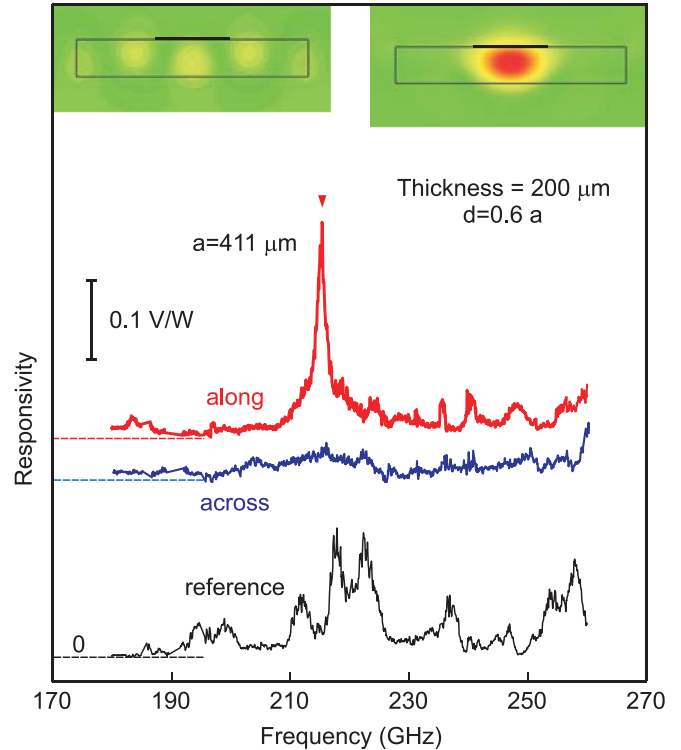


FIG. 2. (Color online) Detector photoresponse versus incident radiation frequency for (upper and middle curves) the sample with PC period $a = 411 \mu\text{m}$ and (lower curve) the reference sample without PC structure. For the PC sample, the response is plotted for two polarization directions. Dashed lines indicate zero levels. Inset panels show simulated maps of the electric field at the resonance points in the longitudinal cross section of the PCS ($a = 411 \mu\text{m}$) in perpendicular and (right panel) longitudinal polarization directions. Thick black line indicates position of the detector in the microcavity. THz plane wave radiation enters from the bottom.

simulations and the experimental results, which confirms that we do observe the effect caused by the photonic crystal. The dependence of the resonance frequency on the inverse period is not linear. That results from the fact that though the hole size of the photonic crystal scales proportionally to the period, the thickness of the slabs does not. The curvature can be explained qualitative as follows. At high frequency the wavelength is small compared to the slab thickness $200 \mu\text{m}$ and the electromagnetic field is concentrated inside the dielectric core of the photonic crystal slab. In this case the effective refractive index is close to the refractive index of GaAs. On the other hand, at lower frequency and correspondingly large wavelength the field spreads out of the dielectric. Hence, the effective refractive index of the system decreases and the resonance frequency becomes smaller than for an infinite 2D photonic crystal. The presented experimental results show that an inherently broadband detector embedded in the PCS microcavity obtains frequency selectivity. Therefore, a set of detectors with photonic crystals tuned to a specific frequency may serve as a spectrometer-on-a-chip for terahertz radiation.

The right inset to Fig. 3 shows detector photoresponse as a function of incident radiation frequency for a PCS with lattice constant $a = 374 \mu\text{m}$ and diameter of air holes $d = 0.4a$, i.e., smaller than in the main figure. It shows, first, that the

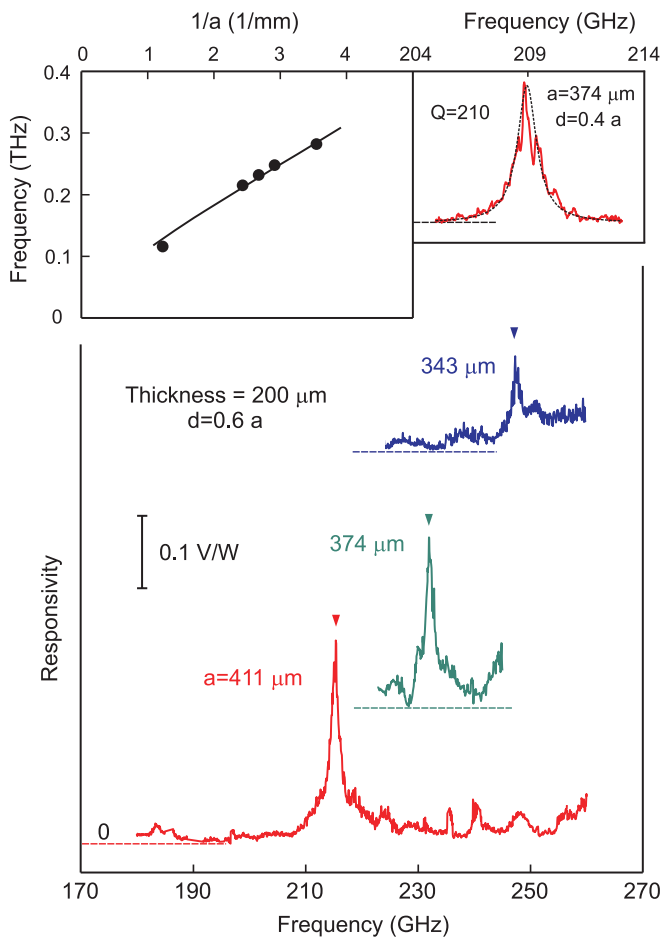


FIG. 3. (Color online) Detector photovoltage as a function of radiation frequency for PCs with periods $a = 411 \mu\text{m}$, $374 \mu\text{m}$, and $343 \mu\text{m}$, thickness $h = 200 \mu\text{m}$, and air hole diameter $d = 0.6a$. Arrows indicate positions of PC resonances. Curves are offset vertically for clarity. Left inset shows resonance frequency as a function of the inverse period $1/a$ of the PC. Right inset displays the frequency dependence of the photoresponse for the PC with a period $a = 374 \mu\text{m}$ and air hole diameter $d = 0.4a$. $Q = 210$ is achieved.

resonance frequency undergoes frequency redshift compared to the case of a $d = 0.6a$ PC slab. Decrease of hole diameter results in increase of microcavity size, and in turn in reduction of resonance frequency from $f = 231 \text{ GHz}$ to 209 GHz . Second, the dashed line represents a Lorentzian fit to the resonant contour, which yields $Q = 210$. It has to be noted that the observed quality factors in our experiment vary from sample to sample. Presumably this is due to the structural nonuniformity of PCSs under study and wave scattering from the sample boundaries. Detailed study of all factors that determine microcavity Q factor is a subject of our further research. Finally, the observed photonic crystal stop band (not shown in the figure) is $\Delta f = 18 \text{ GHz}$ for this sample, which is much smaller than the $\Delta f \approx 50 \text{ GHz}$ stop band for a PCS with $d = 0.6a$. The diameter of the air holes is expected to have a crucial effect on the width of the photonic crystal stop band. The experimentally observed stop band width quantitatively agrees with theoretical calculations,¹⁸ and according to the

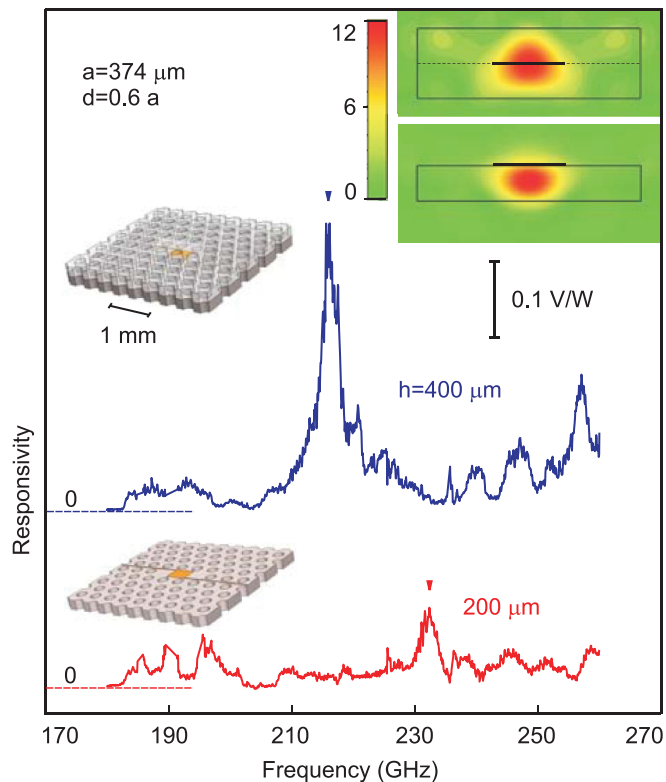


FIG. 4. (Color online) Frequency dependence of photoresponse for (upper curve) detector on top of PC of $h = 0.2 \text{ mm}$ and (lower curve) inside of PC of double thickness $h = 0.4 \text{ mm}$. PC period $a = 374 \mu\text{m}$; hole diameter $d = 0.6a$. Curves are offset for clarity. Inset shows the simulated spatial distributions of the electric field (scale in arbitrary units) in the longitudinal cross section of the PC microcavity for both cases. THz radiation enters from the bottom of the inset; thick black line indicates the position of the detector.

theory the stop band disappears completely for PC slabs with air hole diameter $d = 0.17a$.

At the resonance, the electric field is concentrated mainly inside the dielectric core of the PCS wafer (see inset panels in Fig. 2), which produces an effect that is important for interaction between the resonance photon mode of the microcavity and the detector. The detector, located at the surface of the crystal, senses only the tail of the electromagnetic field, greatly reducing its effectiveness. One of the ways to verify this phenomenon is to place the detector into the center of the dielectric PC slab. This experimental configuration was achieved by placing one photonic crystal on top of another identical one (Fig. 4). The crystals were aligned better than $20 \mu\text{m}$ and glued together at the corners; the resulting air gap between the wafers was also no more than $20 \mu\text{m}$. The bottom curve in Fig. 4 shows the photoresponse of the detector located at the surface of the microcavity in the PC with period $a = 374 \mu\text{m}$ and thickness $h = 200 \mu\text{m}$. The top curve corresponds to the photoresponse of the detector located in between two identical photonic crystals ($a = 374 \mu\text{m}$, total thickness $h = 400 \mu\text{m}$). The amplitude of the resonance increases significantly when the detector is placed in the center of the dielectric PCS. The redshift of the resonance frequency is caused by the change in the PCS thickness from $200 \mu\text{m}$ to $400 \mu\text{m}$ and is in agreement with simulations. The inset

shows results of the theoretical simulation for the electric field amplitude profile in the longitudinal cross-section of the PCS microcavities under study at corresponding resonance frequencies. When we move the detector from the center of the $h = 400 \mu\text{m}$ PC slab to the surface of the $h = 200 \mu\text{m}$ crystal, theory predicts a factor of 4 reduction of the electromagnetic field power density. This prediction is indeed confirmed in the experiment (Fig. 4). The resonances in Fig. 4 have Q factors of about 80. Such low cavity finesse value is due to structural nonuniformity of the PCS used in this experiment.

In summary, we measured photoresponse of a detector embedded in the microcavity in a 2D photonic crystal slab illuminated by sub-terahertz plane-wave radiation propagating perpendicularly to the PCS plane. High- Q resonances were observed in frequency dependence of the photoresponse. It was demonstrated that the resonances originate from coupling

of the microcavity photonic mode to the detector. We have studied the effect of the photonic crystal lattice period, hole size, and detector location on the resonant photoresponse. Theoretical FDTD simulations were found to be in good agreement with experimental data. Our experimental results demonstrate frequency selectivity of a system of integrated detector and PCS produced in one lithographic process. A set of such detectors with photonic crystals tuned to different frequencies may be used to produce a spectrometer-on-a-chip for sub-terahertz and terahertz waves.

Financial support of this work by the Russian Foundation for Basic Research, the Russian Academy of Sciences, and the President of the Russian Federation is gratefully acknowledged.

¹X.-C. Zhang and Jingzhou Xu, *Introduction to THz Wave Photonics* (Springer, New York, 2010).

²E. Yablonovitch, *Phys. Rev. Lett.* **58**, 2059 (1987).

³S. John, *Phys. Rev. Lett.* **58**, 2486 (1987).

⁴J. D. Joannopoulos, P. R. Villeneuve, and S. Fan, *Nature (London)* **386**, 143 (1997).

⁵W. M. Robertson, G. Arjavalingam, R. D. Meade, K. D. Brommer, A. M. Rappe, and J. D. Joannopoulos, *Phys. Rev. Lett.* **68**, 2023 (1992).

⁶M. C. Wanke, O. Lehmann, K. Muller, Q. Wen, and M. Stuke, *Science* **275**, 1284 (1997).

⁷Y. Akahane, T. Asano, B.-S. Song, and S. Noda, *Nature (London)* **425**, 944 (2003).

⁸T. Tanabe, M. Notomi, E. Kuramochi, A. Shinya, and H. Taniyama, *Nat. Photonics* **1**, 49 (2007).

⁹S.-Y. Lin, V. M. Hietala, S.-K. Lyo, and A. Zaslavsku, *Appl. Phys. Lett.* **68**, 3233 (1996).

¹⁰F. Gadot, A. de Lustrac, J.-M. Lourtioz, T. Brillat, A. Ammouche, and E. Akmansoy, *J. Appl. Phys.* **85**, 8499 (1999).

¹¹Z. Jian, J. Pearce, and D.-M. Mittleman, *Opt. Lett.* **29**, 2067 (2004).

¹²Y. Zhao and D. R. Grischkowsky, *IEEE Trans. Microw. Theory Tech.* **55**, 656 (2007).

¹³C. M. Yee and M. S. Sherwin, *Appl. Phys. Lett.* **94**, 154104 (2009).

¹⁴H. Zhang, L. A. Dunbar, G. Scalari, R. Houdre, and J. Faist, *Opt. Express* **15**, 16818 (2007).

¹⁵Y. Chassagneux, R. Colombelli, W. Maineult, S. Barbieri, H. E. Beere, D. A. Ritchie, S. P. Khanna, E. H. Linfield, and A. G. Davies, *Nature (London)* **457**, 174 (2009).

¹⁶V. M. Muravev and I. V. Kukushkin, *Appl. Phys. Lett.* **100**, 082102 (2012).

¹⁷W. Knap, M. Dyakonov, D. Coquillat, F. Teppe, N. Dyakonova, J. Łusakowski, K. Karpierz, M. Sakowicz, G. Valusis, D. Seliuta, I. Kasalynas, A. Fatimy, Y. M. Meziani, and T. Otsuji, *J. Infrared Millim. THz Waves* **30**, 1319 (2009).

¹⁸J. N. Winn, R. D. Meade, and J. D. Joannopoulos, *J. Mod. Opt.* **41**, 257 (1994).